Molecular dynamics of nanodroplet impact: The effect of the projectile's molecular mass on sputtering

Fernan Saiz and Manuel Gamero-Castaño

Citation: AIP Advances **6**, 065319 (2016); doi: 10.1063/1.4954740
View online: http://dx.doi.org/10.1063/1.4954740
View Table of Contents: http://scitation.aip.org/content/aip/journal/adva/6/6?ver=pdfcov
Published by the AIP Publishing

Molecular dynamics of nanodroplet impact: The effect of the projectile's molecular mass on sputtering

Fernan Saiz[1] and Manuel Gamero-Castaño[2,a]
[1]*Department of Chemistry, Imperial College of Science, Technology and Medicine, South Kensington, London, SW7 2A7, United Kingdom*
[2]*Department of Mechanical and Aerospace Engineering, University of California, Irvine, California, 92697, USA*

(Received 31 March 2016; accepted 13 June 2016; published online 20 June 2016)

The impact of electrosprayed nanodroplets on ceramics at several km/s alters the atomic order of the target, causing sputtering, surface amorphization and cratering. The molecular mass of the projectile is known to have a strong effect on the impact phenomenology, and this article aims to rationalize this dependency using molecular dynamics. To achieve this goal, the article models the impact of four projectiles with molecular masses between 45 and 391 amu, and identical diameters and kinetic energies, 10 nm and 63 keV, striking a silicon target. In agreement with experiments, the simulations show that the number of sputtered atoms strongly increases with molecular mass. This is due to the increasing intensity of collision cascades with molecular mass: when the fixed kinetic energy of the projectile is distributed among fewer, more massive molecules, their collisions with the target produce knock-on atoms with higher energies, which in turn generate more energetic and larger numbers of secondary and tertiary knock-on atoms. The more energetic collision cascades intensify both knock-on sputtering and, upon thermalization, thermal sputtering. Besides enhancing sputtering, heavier molecules also increase the fraction of the projectile's energy that is transferred to the target, as well as the fraction of this energy that is dissipated. [http://dx.doi.org/10.1063/1.4954740]

I. INTRODUCTION

The energetic impact of electrosprayed nanodroplets on ceramics and semiconductors causes sputtering, surface amorphization and cratering.[1,2] A nanoprojectile does not penetrate deep into the target, and deposits its kinetic energy in a thin layer below the surface. A significant fraction of this energy is dissipated.[3] In this respect nanodroplets are similar to cluster ions,[4] and differ from smaller atomic projectiles characterized by deep penetration. Electrosprayed nanodroplets are generated as relatively monodisperse beams, their average diameters are controllable from a few to hundreds of nanometers, and are charged near the maximum level set by the Rayleigh limit for liquid droplets.[5] This makes it possible to study energetic impact as a function of projectile diameter from a few nanometers to macroscopic sizes, a size range previously inaccessible due to the lack of a suitable projectile source.[6] A large number of liquids with diverse physical and chemical properties can be electrosprayed, increasing the versatility of nanodroplet beams for fundamental research and applications.

We have recently found that the sputtering yield and the cratering of single-crystal silicon bombarded by nanodroplets is a function of the projectile's molecular mass.[7] These experiments indicate that liquids with low molecular mass like formamide and ethylammonium nitrate, EAN, have a lower sputtering efficiency than liquids with higher molecular mass such as 1-ethyl-3-methylimidazolium

[a]Corresponding author, mgameroc@uci.edu

tetrafluoroborate (EMI-BF_4), 1-ethyl-3-methylimidazolium bis (trifluoro-methylsulfonyl) imide (EMI-Im), triethylsulfoniumbis(trifluoromethylsulfonyl) imide, and trihexyltetrade-cylphosphonium bis(2,4,4-trimethylpentyl) phosphinate. Furthermore, while the impact of the projectiles with higher molecular mass produces micron-sized craters in a range of impact velocities, the surface bombarded by the lower molecular mass projectiles is made only of nanometric indentations at all impact velocities. The different outcomes for projectiles that are otherwise macroscopically identical (same diameters and kinetic energies), points to the importance of molecular level interactions.

This article is a molecular dynamics study of the effect of the molecular mass on the phenomenology of the impact, aimed at rationalizing the experimental findings. Four projectiles with identical radii are considered, made of pseudo atoms with the masses of the molecules of formamide, EAN, EMI-BF_4, and EMI-Im. In each case we adjust the separation of the pseudo atoms to reproduce the density of the liquid, and the impact velocities to make the kinetic energy and stagnation pressure of the projectiles identical. The positions and velocities of the pseudo atoms are analyzed to identify knock-on atoms resulting from the initiation and propagation of collision cascades, to track the energetic state of the area surrounding the impact, and ultimately to establish a connection between molecular mass and sputtering. The simulations confirm that projectiles with larger molecular mass produce more energetic collision cascades and higher thermal fields in the area of the impact, and therefore higher sputtering by knock-on atoms and thermal evaporation.

II. SIMULATION METHODS

We use the molecular dynamics package LAMMPS to model the impact of a nanodroplet on single-crystal silicon.[8] The droplet has a diameter D of 10 nm, and is made of identical spheres arranged in a hexagonal close-packed array. Each sphere represents the molecule of a liquid (formamide, EAN, EMI-BF_4 and EMI-Im), with radius and mass set to match the liquid's density and molecular mass. The simulation treats the spheres as pseudo atoms, i.e. as point masses that interact with other atoms through prescribed potentials. We do not simulate individual atoms within the molecule, and therefore potential phenomena such as molecular dissociation and molecular degrees of freedom are not considered. The (100) Si target is a slab 36.5 nm deep in the impact direction, 48.8 nm wide in the lateral directions, and filled with 4,390,200 Si atoms in the standard cubic-diamond lattice. Prior to the impact the slab is relaxed with a 293K Berendsen thermostat applied to its boundaries for 20 ps. The thermostat is maintained on the lateral and bottom faces throughout the impact, to prevent the unphysical reflection of shock waves at the boundaries.[3,9] The projectile is directed towards the target at velocity v_P, and the equations of motion are integrated during 70 ps with a timestep of 1 fs. The impact velocities are adjusted so that all projectiles have an identical kinetic energy of 63 keV, and a stagnation pressure of 19 GPa, $P_0 = \rho v_P^2/2$. To facilitate the comparison between different projectiles we will use the characteristic time $t_C = D/v_P$ as the unit of time in most figures. Table I collects the density and molecular mass of the liquids, the radius of the spheres, the number of spheres, the impact velocity and the characteristic time for each projectile. The molecular masses range between 45.0 and 391.3 amu, and the impact velocities between 5.87 and 5.00 km/s. The associated molecular kinetic energies for the formamide, EAN, EMI-BF_4 and EMI-Im projectiles are 8.03, 17.12, 30.54, and 50.69 eV respectively.

The forces between silicon atoms are calculated with the Stillinger-Weber potential.[10] This potential accurately reproduces the crystalline and liquid phases, and the normal melting point of

TABLE I. Density ρ (kg/m^3), molecular mass m_m (amu), simulated molecular radius r_m (nm), number of molecules N_m , impact velocity v_P (km/s), and characteristic time of the impact t_C (ps), for the four projectiles.

Liquid	ρ	m_m	r_m	N_m	v_P	t_C
Formamide	1130	45.04	0.227	7845	5.87	1.70
EAN	1261	108.09	0.293	3682	5.53	1.81
EMI-BF_4	1294	197.97	0.366	2064	5.46	1.83
EMI-Im	1520	391.31	0.422	1243	5.00	2.00

Si. It has been used extensively to capture the amorphization of silicon by fast quenching of a melt, and to calculate the sputtering yield associated with atomic and cluster ion bombardment.[11–13] The forces between the projectile's pseudo atoms, and between the pseudo atoms and the Si atoms are calculated with the Ziegler-Biersack-Littmark (ZBL) potential, using the aggregate atomic number of the atoms in the molecule as the atomic number in the ZBL parametrization.[14] The following two arguments justify this simplified model: the projectile molecules are expected to remain largely intact due to the relatively low impact energy per atom (impact simulations of fullerene projectiles have shown that as much as 8.3 eV per C atom is required to promote significant atom dissociation);[15] and previous simulations of nanodroplet impact using the ZBL potential reproduce experimental sputtering yields, as well as the onset and extent of amorphization.[3,16]

The impact of each projectile is simulated five times to average results whenever appropriate. We apply the methodology proposed by Samela and Nordlund to identify knock-on atoms produced by direct collisions with projectile molecules, and by collision cascades of Si atoms.[17] To identify knock-on atoms we store the positions and velocities of the atoms in the neighborhood of the impact every 2 fs, during the first 10 ps of the impact. This period is long enough to identify practically all the primary (PKA), secondary (SKA), and tertiary (TKA) knock-on atoms. An atom is classified as PKA if at some point its kinetic energy exceeds 0.50 eV, and there is a molecule of the projectile in its neighborhood when it first reaches this level. SKA and TKA are similarly defined, but they must have a PKA and an SKA in the neighborhood respectively. The actual choice for the energy threshold is arbitrary, and we use 0.50 eV because this is the energy required to heat silicon from 293 K to its melting point (0.18 eV), and melt it (the melting enthalpy predicted by the Stillinger-Weber potential is 0.32 eV).[18] We have tested different threshold energies between 0.5 eV and the 0.1 eV value proposed by Samela and Nordlund, and confirmed that although the total number of knock-on atoms is affected by the choice, the conclusions of the analysis are not. A particle is defined to be in the neighborhood of a Si atom if it is found within a radius of 3 Å. This distance, slightly longer than the 2.4 Å of the nearest neighbor shell in the Si crystal, allows counting knock-on atoms produced by many-body collisions.

III. IMPACT PHENOMENOLOGY

Figure 1 shows a thin slice of the target and the projectile for the four molecular masses, near $t/t_C = 1$. The projectile impacts on the surface at $t/t_C = 0$. The pseudo atoms of the projectile are shown in white, and silicon atoms are in a color scale indicating the thermal energy per atom, $3\,k_B T/2$, where the temperature is evaluated at the position of the atom. The temperature at a point is defined as

$$T = \frac{m \sum_{i=1}^{N} (\mathbf{v}_i - < \mathbf{v}_i >)^2}{3k_B N} \tag{1}$$

where N atoms are enclosed in a spherical control volume centered at the point, k_B is the Boltzmann's constant, m is the atomic mass of silicon, and $\mathbf{v}_i$ is the velocity vector of the i-atom. Eq. (1) can also be used to define a pseudo temperature in the absence of partial thermodynamic equilibrium. The fields in Fig. 1 are obtained with control volumes 1.36 nm in radius typically containing 524 atoms, a number large enough to compute reliable statistics. Fig. 1 shows that the dissipation of the projectile's energy gradually increases with molecular mass: while formamide and EAN generate a thin layer of atoms with peak thermal energies below 0.85 eV, the impact of the EMI-BF_4 and EMI-Im projectiles produce thicker hot layers with peak values up to 4.73 eV. Although EMI-BF_4 seems to generate a hot layer thicker than EMI-Im, this is just an artifact of the plot: the EMI-Im molecules penetrate slightly on the target, blocking the view of a considerable number of red Si atoms. Figure 2 shows a second snapshot at a slightly later time, $t/t_C \cong 2.5$. Although the four impacts display a melted band surrounding the impact (the normal melting point of Si, 1685 K, corresponds to a thermal energy of 0.218 eV), the temperature field within this band barely exceeds the melting point in the case of formamide, and increases with molecular mass for EAN, EMI-BF_4 and EMI-Im. Furthermore the crater shifts gradually from a smooth and

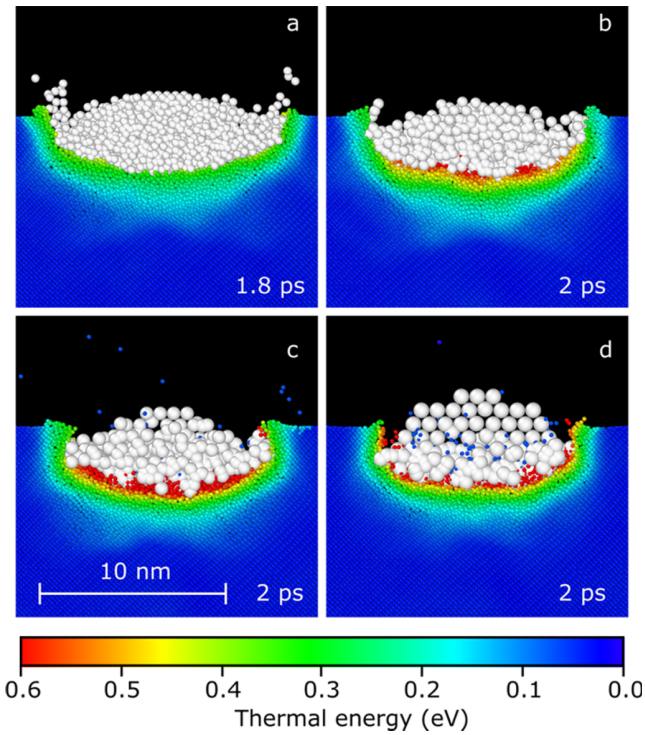

FIG. 1. Cross sections of the impact region at times near t_C for formamide (a), EAN (b), Emi-BF_4 (c), and Emi-Im (d).

axisymmetric ellipsoidal shape in the case of formamide to a more irregular and deeper hemisphere in the case of Emi-Im. The maximum depth of the crater is 5.4 nm for formamide, 6.1 nm for EAN, 6.5 nm for EMI-BF_4, and 7.2 nm for EMI-Im, and is reached at $t/t_C \cong 2.5$. After this point the surface oscillates until the depth settles at 1.8nm for formamide, 2.6 nm for EAN, 3.8 nm for

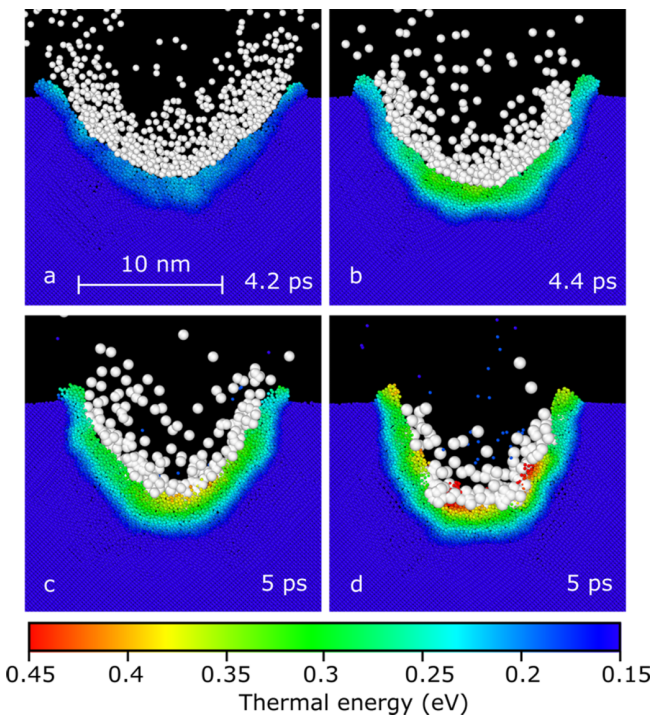

FIG. 2. Cross sections of the impact region at times near $2.5t_C$ for formamide (a), EAN (b), Emi-BF_4 (c), and Emi-Im (d).

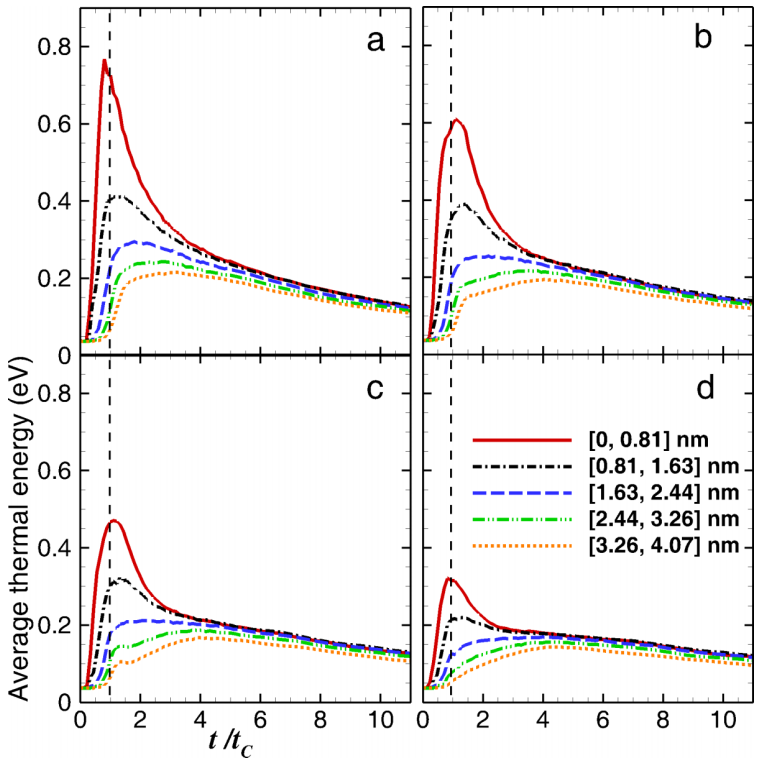

FIG. 3. Evolution of the average thermal energy per atom at varying depth for the EMI-Im (a), EMI-BF_4 (b), EAN (c), and formamide (d) projectiles.

EMI-BF_4, and 5.6 nm for EMI-Im. At $t/t_C \cong 15$ the region surrounding all four impacts undergoes a liquid to amorphous transition resulting from an ultrafast quench.

Figure 3 plots the average thermal energy per atom as a function of time and distance from the surface. To obtain these curves we divide the area surrounding the crater into sequential layers 0.81 nm thick, and divide the thermal energy of the layer by the number of atoms it contains. The shapes of the curves are similar for all projectiles: the thermal energy in any layer initially increases; it reaches a maximum value that decreases with depth, at a time that increases with depth; the maximum value for the outermost layers is located at $t/t_C \cong 1$, as indicated by the dashed lines inserted in the figures; and the energy gradient is initially rather intense, and decreases significantly beyond $t/t_C \gtrsim 3$. On the other hand the molecular mass has a very strong effect on the height of the curves, the higher the molecular mass the more elevated the average thermal energy and therefore the larger the fraction of the projectile's energy that is dissipated. For example, the maximum value of the average energy in the outermost layer is 0.77, 0.61, 0.47 and 0.32 eV for EMI-Im, EMI-BF_4, EAN and formamide respectively.

Figure 4 shows the evolution of the projectile's kinetic energy E_K, and how this energy is transferred to the target and converted into translational E_{CM}, thermal E_{Th}, and potential E_P energies. All energies are scaled with the initial kinetic energy of the projectile, and the thermal and potential energies are offseted with their initial values. To calculate the target energies we divide it in adjacent cubical volumes 1.69 nm in side, compute the energy of each volume, and add them up. The translational energy of the k volume is given by:

$$E_{CM}^k = \frac{1}{2} N^k m < \mathbf{v}_i >^2 \tag{2}$$

where N^k is the number of Si atoms in the volume; its thermal energy is:

$$E_{Th}^k = \frac{m}{2} \sum_{i=1}^{N^k} (\mathbf{v}_i - < \mathbf{v}_i >)^2 \tag{3}$$

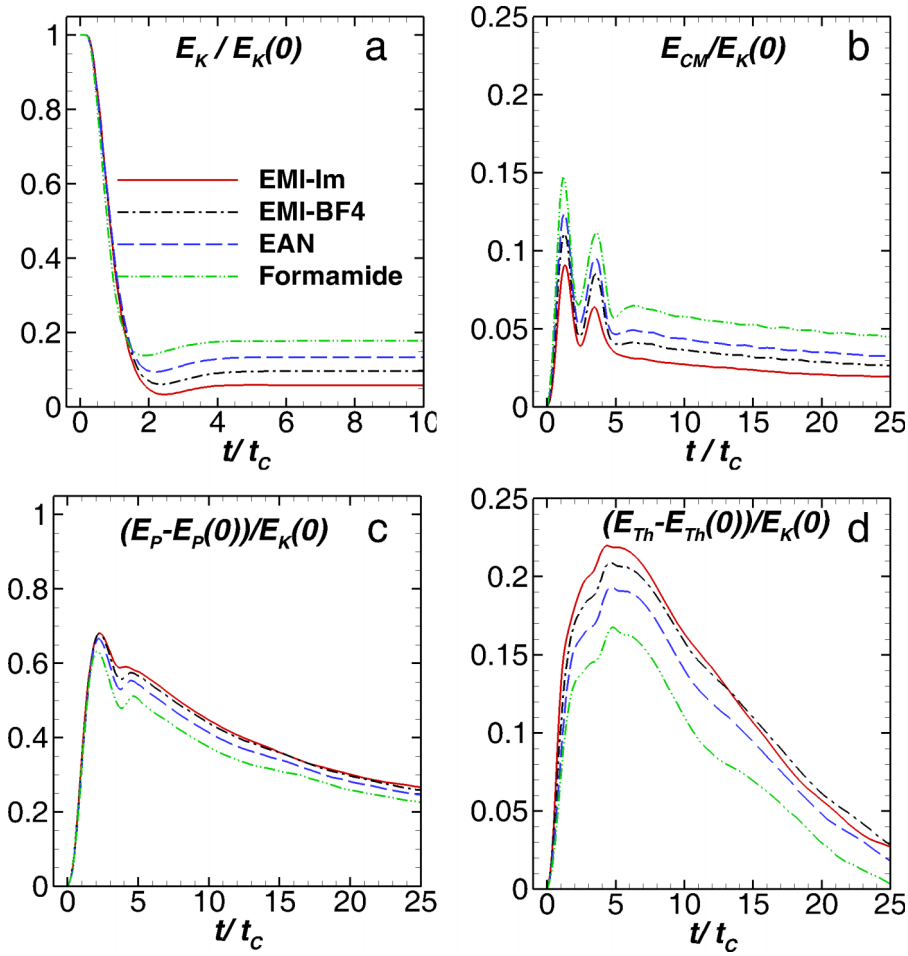

FIG. 4. Kinetic energy of the projectile (a), and translational (b), potential (c), and thermal (d) energies of the target as a function of time.

and the potential energy is the sum of the potential energies of the N^k atoms. Fig. 4(a) shows that all impacts are characterized by a brief phase of intense collisionality, $t/t_C \lesssim 2$, within which most of the kinetic energy of the projectile is transferred to the target. The efficiency of this transfer increases with molecular mass, for example by the end of the simulation the molecules of formamide, EAN, EMI-BF_4 and EMI-Im retain 17.7%, 13.3%, 9.5% and 5.9% of their initial kinetic energy. The translational energy of the targets in Fig. 4(b) peaks at $t/t_C \cong 1.25$, with maximum values between 9.1% and 14.7% of the impact energy for EMI-Im and formamide respectively; it rebounds at $t/t_C \cong 4$ to produce a second lower peak, associated with the unloading of the target following the absorption of the projectile's momentum; and finally asymptotes to values between 1.8% for EMI-Im and 4.1% for formamide, as the target is left with a small and uniform constant velocity. Figure 4(c) shows that in the initial phase of the impact the largest fraction of the projectile's energy is converted into potential energy, peaking at a value between 63.3% for formamide and 68.1% for EMI-Im. The potential energy then decays, first in an initial abrupt step associated with the unloading and decompression of the target, $2 \lesssim t/t_C \lesssim 5$, followed by a progressively decreasing rate as the molten silicon cools down and solidifies, producing a phase of lower potential energy. The fully relaxed target maintains an excess potential energy between 23.8% and 19.3% of the impact energy for EMI-Im and formamide respectively, associated with the formation of defects and of an amorphous layer surrounding the crater. Finally, Fig. 4(d) shows how the thermal energy of the targets increases sharply in the initial stage of the impact, peaking at $t/t_C \cong 4.7$ between 21.9% for EMI-Im and 16.7% for formamide, which is followed by a decay towards thermal equilibrium

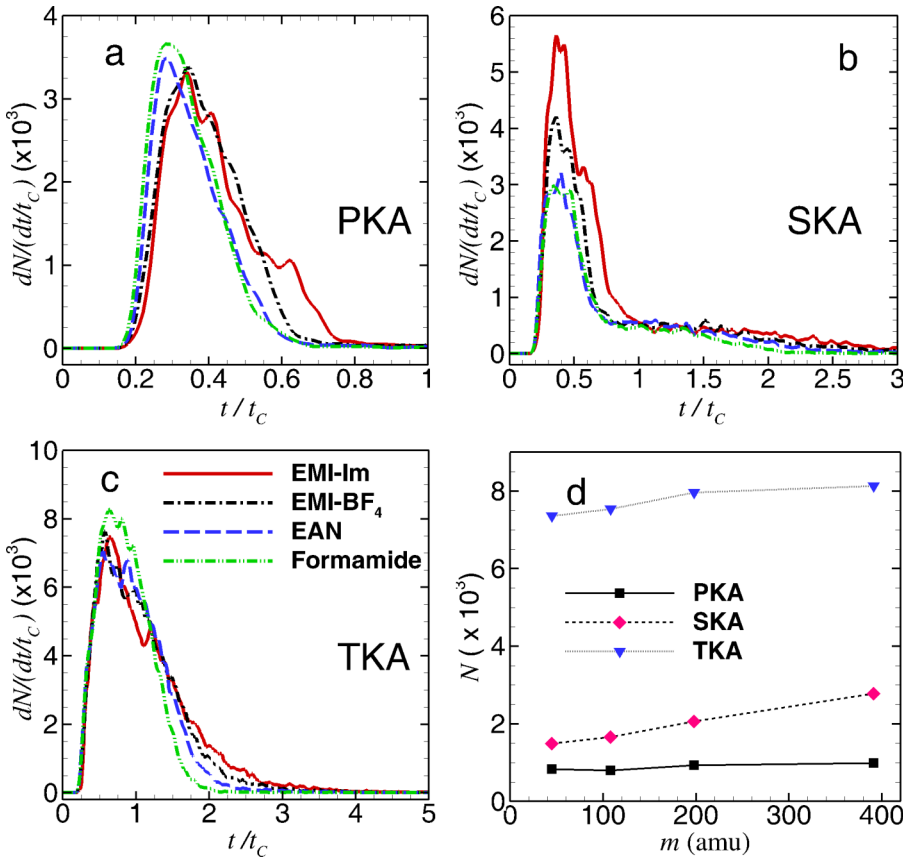

FIG. 5. Rate at which primary (a), secondary (b) and tertiary (c) knock-on atoms are produced. (d) total numbers of knock-on atoms as a function of molecular weight.

as heat is removed by the walls. Three features of the curves are worth highlighting: the fraction of the projectile's kinetic energy that is dissipated is significant; this fraction increases with molecular mass; and most of the thermal energy is deposited in a thin layer surrounding the impact, as can be inferred from the short time needed to reach the maxima.

Figures 5(a)–5(c) show the rates at which primary, secondary and tertiary knock-on atoms are generated, and Fig. 5(d) shows their total numbers. PKAs are generated early in the impact, $t/t_C \lesssim 0.6$, significantly before the projectile ceases transferring energy at $t/t_C \cong 2$; SKAs are generated in two distinct periods, one mirroring the formation of PKAs and a second, more protracted period extending up to $t/t_C \cong 2.5$; and TKAs are generated more uniformly throughout $t/t_C \lesssim 2.5$. The total number for each type of knock-on atom increases moderately with molecular mass and, at least up to the third generation level (PKA→SKA→TKA), each generation is produced in increasing numbers; depending on the molecular mass, the ratios between the total numbers of SKAs and PKAs, and TKAs and SKAs, vary between 1.8 and 2.8, and 4.9 and 2.0 respectively. This information is complemented with the evolution of the average kinetic energies in Fig. 6. Only results for the heavier and lighter molecule are given for clarity, and the data for the other two molecular masses fall monotonically in between these two extremes. The average kinetic energies peak at $t/t_C \cong 1$, and rapidly decrease thereafter so that by $t/t_C \cong 3$ all knock-on atoms are largely thermalized with the surrounding atoms. For a given impact PKAs are more energetic than SKAs, while TKAs have the lowest energies. The key piece of information in this figure is that the maximum kinetic energies increase significantly with the projectile's molecular weight, especially for the PKA and SKA populations. For example, the energy of PKAs peaks at 0.99 eV for formamide, 1.17 eV for EAN, 1.73 eV for EMI-BF_4, and 2.08 eV for EMI-Im. This is due to the larger momentum of the heavier molecules, and therefore to the increased value of the energy

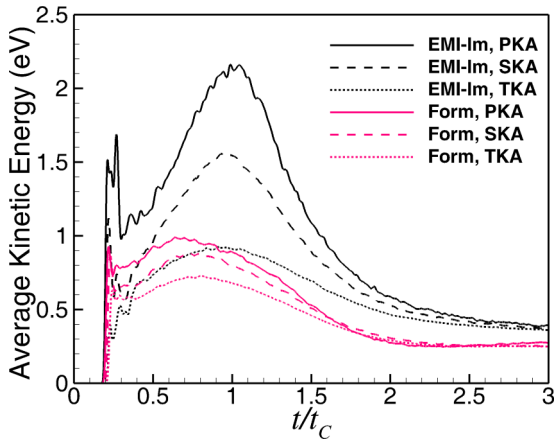

FIG. 6. Evolution of the average kinetic energies of knock-on atoms for EMI-Im and formamide.

that is transferred to silicon atoms within the first few collisions. These figures also reveal the lack of penetration of the molecules: the thickness of the region in which the energy of the projectile is transferred can be estimated with the total number of PKAs, the atomic density of Si, and an area of impact equal to the cross section of the projectile. For an average number of 886 PKAs, the resulting thickness is 0.22 nm, i.e. only 41% of the lattice parameter. Since the molecules do not penetrate deeper, the energy of the projectile that continues being transferred in the $0.6 \lesssim t/t_C \lesssim 2$ window is not invested in producing a larger number of PKAs, but on further energizing the existing thin layer of PKAs. This is reflected in the increasing average energy of PKAs beyond $t/t_C \cong 0.8$, i.e. long after these atoms stop being generated. Another interesting feature is the rapid thermalization of the collision cascades, as indicated by the distinct protracted period of formation characteristic of the second generation of knock-on atoms, the uniform formation of TKAs, and the convergence of the average energies for $t/t_C \gtrsim 2$.

Figure 7 plots the sputtering rates Y' and the average energy $<\varepsilon>$ of sputtered atoms for EMI-Im and EMI-BF_4, as a function of time. EAN only ejects 3 atoms on average, while formamide does not eject any. Table II collects the total number of ejected atoms, the fractions of ejected atoms that are PKAs, SKAs and TKAs, and their energy averages and standard deviations. The main feature is that the sputtering increases strongly with molecular mass; in addition, all PKAs, SKAs and TKAs are ejected in meaningful quantities. The average energies of the ejected PKAs and SKAs are similar, and comparable to the surface binding energy of silicon (estimated to be 4.67 eV, the value of the standard enthalpy of formation of Si(g)),[19] while the average energies of the ejected TKAs are smaller; this is consistent with the lower fraction of ejected TKAs respect to their total numbers. Fig. 7 shows that most of the sputtering takes place early in the impact, $t/t_C \lesssim 1.25$, i.e. when the average energy of the outermost layer of silicon atoms peaks (see Fig. 3), and before the projectile has finished transferring its energy at $t/t_C \lesssim 2$. The sputtering rate also correlates well with the average energy of the ejected atoms, as indicated by the similar shapes of the Y' and $<\varepsilon>$ curves. Clearly, in this initial and most intense sputtering phase the ejection of atoms is driven by energetic collisions with both the molecules of the projectile and with energetic silicon atoms, in the absence of local equilibrium. Since the average energy of the atoms in the impact region, and in particular near the surface, increases with the molecular mass of the projectile, the sputtering rate is strongly correlated with molecular mass. In addition to this knock-on sputtering, a smaller number of atoms with lower average energies are ejected in a second phase around $t/t_C \cong 2$. By this time the most energetic molecule/atom and atom/atom collisions have subsided, and since the average energies of PKAs, SKAs and TKAs have largely converged, the surface is approaching local thermodynamic equilibrium and the ejection can be described as thermal sputtering. Because the dissipation of the energy of the impact and the associated temperature field increase with molecular mass, thermal sputtering also increases with molecular mass.

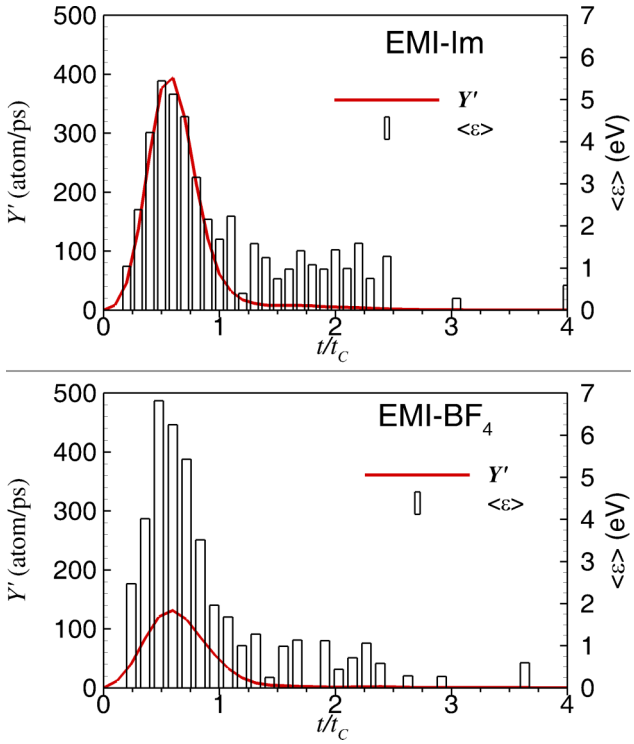

FIG. 7. Sputtering rate and average energy of ejected atoms for EMI-Im and EMI-BF_4.

TABLE II. Average number of ejected atoms N, percentage that are PKAs, SKAs and TKAs, and their energy averages and standard deviations $<\varepsilon>/\sigma$.

Liquid	N	*PKA (%)*	$<\varepsilon>/\sigma_{PKA}$	*SKA (%)*	$<\varepsilon>/\sigma_{SKA}$	*TKA (%)*	$<\varepsilon>/\sigma_{TKA}$
EMI-Im	410	31.6	4.5 / 3.6	44.3	4.5 / 3.8	24.1	2.2 / 3.2
EMI-BF_4	144	45.6	5.5 /4.5	37.6	4.9 / 4.8	16.8	2.1 / 3.7

IV. CONCLUSIONS

The molecular mass of a nanoprojectile has a strong effect on the outcome of the impact. Increasing the molecular mass at fixed projectile diameter and kinetic energy causes higher energy dissipation and temperature fields in the target, as well as sputtering. The fundamental reasons for this is the increasing intensity of collision cascades with molecular mass: when the fixed kinetic energy of the projectile is distributed among fewer, more massive molecules, their collisions with the target produce knock-on atoms with higher energies, which in turn generate more energetic and larger numbers of secondary and tertiary knock-on atoms. The effect on sputtering is twofold: first, in knock-on sputtering only atoms with energies comparable to the surface binding energy are ejected in significant numbers, and massive molecules produce more atoms that can overcome this energy hump; and second, the thermalization of more energetic collision cascades produces higher dissipation and temperatures, and therefore higher thermal sputtering. Knock-on sputtering is the dominant sputtering mechanism at the conditions simulated in this work.

The low penetration of the molecules in the target is an important characteristic of nanoparticle impact, and a unique method for depositing high energy densities on a thin surface layer. The scaling of molecular penetration, and of the resulting temperature and density fields with the velocity, diameter and molecular mass of the projectile remains to be investigated, and is a natural extension of this work. The study of impact velocities exceeding tens of km/s, and the use of an all-atom model for the molecule, are especially interesting.

[1] R. Borrajo-Pelaez, E. Grustan-Gutierrez, and M. Gamero-Castano, "Sputtering of Si, SiC, InAs, InP, Ge, GaAs, GaSb, and GaN by electrosprayed nanodroplets," J. Appl. Phys. **114**, 184304 (2013).
[2] M. Gamero-Castaño, A. Torrents, R. Borrajo-Pelaez, and J.-G Zheng, "Amorphization of hard crystalline materials by electrosprayed nanodroplet impact," J. Appl. Phys. **116**, 174309 (2014).
[3] F. Saiz and M. Gamero-Castaño, "Atomistic modeling of the sputtering of silicon by electrosprayed nanodroplets," J. Appl. Phys. **116**, 054303 (2014).
[4] I. Yamada and N. Toyoda, "Nano-scale surface modification using gas cluster ion beams. A development history and review of the Japanese nano-technology program," Surf. Coat. Technol. **201**, 8579–8587 (2007).
[5] M. Gamero-Castaño, "Characterization of the Electrosprays of 1-Ethyl-3-Methylimidazolium Bis(Trifluoromethylsulfonyl) Imide in Vacuum," Phys. Fluids **20**, 032103 (2008).
[6] J. Samela and K. Nordlund, "Atomistic Simulation of the Transition from Atomistic to Macroscopic Cratering," Phys. Rev. Lett. **101**, 027601 (2008).
[7] R. Borrajo-Pelaez, F. Saiz, and M. Gamero-Castaño, "The Effect of the Molecular Mass on the Sputtering of Si, SiC, Ge, and GaAs by Electrosprayed Nanodroplets at Impact Velocities up to 17 km/s," Aer. Sci. Tech. **49**, 256-266 (2015).
[8] S. J. Plimpton, "Fast parallel algorithms for short-range molecular-dynamics," J. Comput. Phys. **117**, 1-9 (1995).
[9] J. Samela, J. Kotakoski, K. Nordlund, and J. Keinonen, "A quantitative and comparative study of sputtering yields in Au," Nucl. Instrum. Methods Phys. Res. B **239**, 331–346 (2005).
[10] F. H. Stillinger and T. A. Weber, "Computer-simulation of local order in condensed phases of silicon," Phys. Rev. B **31**, 5262–5271 (1985).
[11] J. Samela, K. Nordlund, J. Keinonen, and V. N. Popok, "Comparison of silicon potentials for cluster bombardment simulations," Nucl. Instr. Meth. Phys. Res. B **255**, 253-258 (2007).
[12] B. J. Thijsse, T. P. C. Klaver, and E. F. Haddeman, "Molecular dynamics simulation of silicon sputtering: sensitivity to the choice of potential," Appl. Surf. Sci. **231**, 29-38 (2004).
[13] Z. Insepov and I. Yamada, "Molecular-dynamics simulation of cluster ion-bombardment of solid-surfaces," Nucl. Instr. Meth. Phys. Res. B **99**, 248-252 (1995).
[14] J. F. Ziegler, J. P. Biersack, and U. Littmark, *The Stopping and Range of Ions in Solids* (Pergamon, New York, 1985).
[15] C. Anders, H. Kirihata, Y. Yamaguchi, and H. Urbassek, "Ranges and fragmentation behavior of fullerene molecules: A molecular-dynamics study of the dependence on impact energy and target material," Nucl. Instrum. Methods Phys. Res. B **255**, 247–252 (2007).
[16] F. Saiz, R. Borrajo-Pelaez, and M. Gamero Castaño, "The influence of the projectile's velocity and diameter on the amorphization of silicon by electrosprayed nanodroplets," J. Appl. Phys. **114**, 034304 (2013).
[17] J. Samela and K. Nordlund, "Emergence of non-linear effects in nanocluster collision cascades in amorphous silicon," New J. Phys. **10**, 023013 (2008).
[18] W. D. Luedtke and U. Landman, "Preparation, structure, dynamics, and energetics of amorphous-silicon - a molecular-dynamics study," Phys. Rev. B **40**, 1164-1174 (1989).
[19] V. G. Sevast'yanov, P. Y. Nosatenkob, V. V. Gorskiib, Y. S. Ezhovc, D. V. Sevast'yanova, E. P. Simonenkoa, and N. T. Kuznetsova, "Experimental and theoretical determination of the saturation vapor pressure of silicon in a wide range of temperatures," Russ. J. Inorg. Chem. **55**, 2073–2088 (2010).